Hindawi
Advances in Civil Engineering
Volume 2022, Article ID 8627124, 14 pages
https://doi.org/10.1155/2022/8627124

Research Article

Settlement Characteristics of Split Grouting Pile Composite Foundation in Loess Areas

Mingru Zhou,[1,2] **Lijun Xing**,[1] **Yiming Chen**,[1] **and Hongxia Qiao**[1,2]

[1]*School of Civil Engineering, Lanzhou University of Technology, Lanzhou 730050, China*
[2]*Gansu Advanced Civil Engineering Materials Engineering Research Center, Lanzhou 730050, China*

Correspondence should be addressed to Mingru Zhou; 1799272765@qq.com

Received 29 August 2022; Revised 3 November 2022; Accepted 10 November 2022; Published 23 November 2022

Academic Editor: Paolo S. Valvo

Loess foundations often affect the stability of superstructures due to their insufficient bearing capacities; thus, reinforcement measures are crucial for mitigating the uneven settlement of foundations. This study aims to investigate the settlement characteristics of composite foundations for loess foundations reinforced by splitting grouting piles. First, split grouting tests were carried out on loess foundations. After the test piles reached the design strength, static load tests and geotechnical tests were carried out to obtain the *Q-s* curves of the test piles. The pile-forming mechanism was analyzed via excavations at an on-site test pile. Furthermore, the traditional settlement calculation method of composite foundations was used to calculate the settlement of split grouting pile composite foundations, and the results were compared with field test results to explore a suitable settlement calculation method of split grouting pile composite foundations. Finally, the numerical model of split grouting pile composite foundations was established according to the pile forming mechanism, and the settlement deformation characteristics of single pile and pile group composite foundations were analyzed. The relative errors of the composite modulus method and the stress correction method for calculating the settlement of the composite foundations were 6.4% and 32.8%, respectively, and the composite modulus method was closer to the test values. The calculated curves of the numerical model were in good agreement with the measured curves and relevant literature research results, demonstrating the rationality of the modeling method; the findings of this study provide theoretical guidance for designing loess foundation splitting grouting reinforcement and for predicting settlement during later construction periods.

1. Introduction

In recent years, with continuous advances in geotechnical engineering theories and test equipment [1], geotechnical engineering reinforcement technologies have developed rapidly. It is mainly divided into anchoring [2, 3] and grouting technologies. The two technologies are not independent but rather inextricably linked. As a foundation reinforcement method, grouting technology has been widely used in practical engineering applications owing to its small influence range during construction, simple operation process, and good effect on the uneven settlement of existing buildings. As a branch of the split grouting technology, shear tests have shown that the split diffusion of grout can significantly improve the shear deformation resistance of soil [4, 5]. At the same time, the pile core stone body formed in a grouting hole can effectively bear the load. Therefore, the composite foundation has good integrity and strong bearing capacity, and thus, it is widely used in various engineering fields such as highways, construction, municipal infrastructure, and water conservation.

Several scholars have extensively investigated composite foundations. Based on the deformation characteristics of rigid piles, Lang and Yang [6] proposed a quasi-equal strain hypothesis to analyze the consolidation characteristics of rigid pile composite foundations and verified the rationality of this hypothesis by comparing theoretical derivation with numerical simulation results. Chen et al. [7] used the equivalent continuum method to simplify a large number of compaction piles in the composite foundation. Relying on

the case of the composite foundation with granular material piles in collapsible loess areas, it was verified that this method can provide novel insights for developing three-dimensional calculation models of composite foundations. Zhu et al. [8] used model tests and numerical simulations to investigate the influence of the proposed constitutive model of the soil on the settlement characteristics of pile raft foundations under cyclic load. Gao et al. [9] used geosynthetics-wrapped stone columns (GESCs) to strengthen soft soil foundations and analyzed the settlement of the new composite foundations and the change of pile-soil stress. Yi et al. [10] studied the bearing capacities and failure modes of composite foundations comprising T-shaped columns, as determined via laboratory model tests. To study the settlement mechanism and influence law, Zhang et al. [11] proposed an analytical solution for investigating the settlement of composite foundations strengthened by stone columns by analyzing the deformation characteristics of stone columns under vertical loads. Liu et al. [12] conducted an experimental study on the performance of steel slag columns wrapped with geosynthetics in soft clay foundations. Useche–Infante et al. [13] investigated the influence of grouting at pile ends and pile sides on the bearing capacities of pile foundations via field tests and theoretical analyses and finite element numerical calculations.

To sum up, while there has been extensive research on the bearing capacity and settlement calculation of composite foundations with other pile types, relatively few studies have focused on split grouting pile composite foundations in the loess area, and there are insufficient relevant theoretical calculations. Based on the field split grouting pile test, in this study, the settlement and bearing performance of composite foundations were analyzed. The finite element method was used to establish the model according to the field test, and the influence of the split branch on the load-deformation was analyzed, providing theoretical guidance for promoting the application of split grouting piles.

2. Principle of Split Grouting Pile Composite Foundations

As determined in [14], the particle size of loess is mainly silted (content = 55%–75%), the particle size is 0.005–0.05 mm, loess density is loose, and there are many large and medium voids (pore diameter, $d > 0.004$ mm); the particle size of ordinary cement is 0–0.15 mm. Due to this difference in particle size, cement slurry cannot easily infiltrate and diffuse in loess, but it can split and diffuse. The grouting process of loess foundation splitting is typically divided into three stages, namely, filling and compacting of loess mass, plastic cracking of loess mass, and crack propagation and formation of slurry plate. After the loess foundation is mechanically formed into holes, with increase in grouting pressure, the slurry squeezes the soil skeleton, and the loess around the hole gradually changes from an elastic state to a plastic state, accompanied by small-scale infiltration and diffusion. According to theoretical calculations, the filling and compaction stages of soil mass obey the circular hole expansion theory, as shown in Figure 1(a). When the grouting pressure increases to a certain level, plastic cracking occurs due to the unstable plastic state, and the soil cracking and crack expansion stages are considered to obey the fracture mechanics theory. The crack development model is I-type, as shown in Figure 1(b).

According to the diffusion mechanism of split grouting [16], the split grouting pile splits the foundation loess through the high-pressure cement slurry with a grouting hole as the center, and it relies on the slurry to split and spread in the loess until it finally solidifies in the foundation to form a cement slurry stone body, achieving improved properties of the loess. Split grouting piles have the characteristics of low-strength piles, and they belong to the category of flexible piles according to the relative stiffness of piles and soils. Field test results show that the split grouting pile comprises a vertical core stone body and a horizontal split grout vein. The grouting slurry chemically reacts with the particles in the loess layer around the grouting hole and hydraulic splitting crack through its own flow characteristics, forming new higher-strength compounds. Due to the cementation effect of the grout, the pile-soil interface bond performance is good after pile formation, and the pile side friction resistance is high, forming a new type of composite foundation with good integrity, as shown in Figure 2.

3. Split Grouting Test

3.1. Site Geology Overview. The test site was located near the South Expressway, Xicha Town, Lanzhou New District. According to the geological survey report, the first layer of the site was artificial backfill soil, which was yellowish-brown and slightly wet and had poor soil uniformity. The soil comprised a small amount of fine sand, along with broken bricks and blocks, most of which were compacted, resulting in an average thickness of 3.2 m. The second layer was loess-like silt, which was light yellow, and it mainly comprised granulated, slightly wet, medium-density, and relatively uniform soil; this soil showed white calcareous stripes, low dry strength, low toughness, and an average thickness of 6.4 m. The third layer was the Malan loess layer, which is yellowish-brown and is dominated by silt particles; the soil was pure and uniform, with large pores and a small number of calcareous streaks; it was slightly wet, had medium density, and had an average thickness of 25 m. The physical properties of the soil layer are shown in Table 1.

3.2. Grouting Design. The test material investigated in this study was PO 42.5 composite silicate cement (Hongshi corporation, Yongdeng County, Gansu Province). Performance indicators of the cement are listed in Table 2. After experimental research on the properties of cement slurry [17], such as specific gravity, 2 h water separation rate, stone rate, and solid body strength and viscosity, the stone body strength of the high water-cement ratio slurry was small, which did not meet the requirements of stone body strength. The high water-cement ratio may cause secondary collapsibility during grouting; a lower water-cement ratio may result in higher strength; however, the viscosity of the slurry

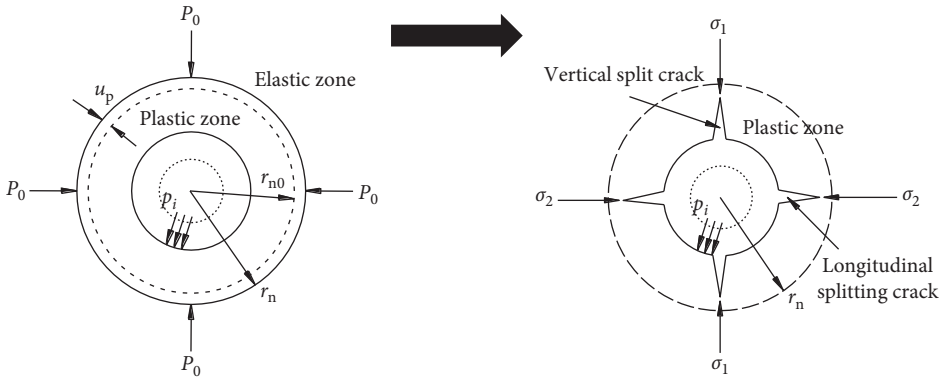

Figure 1: Mechanism of split grouting pile formation.

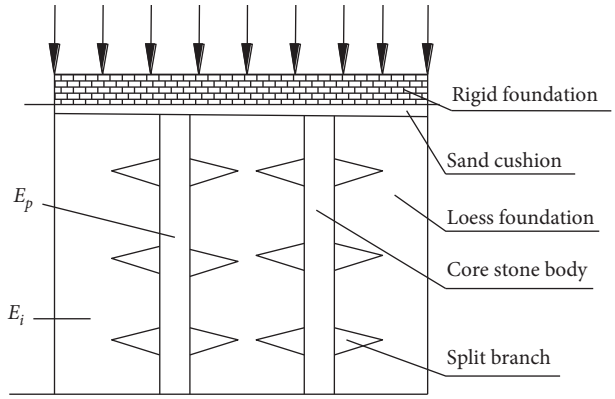

Figure 2: Split grouting pile composite foundation.

Table 1: Soil distribution and parameters.

Soil layer	Thickness (m)	Poisson's ratio	Water content (%)	Density (kN/m^3)	Compression modulus (MPa)
Backfill layer	3.9	0.38	7.8	1.55	5.4
Loess-like silt	7.1	0.32	8.5	1.47	9.0
Malan loess	25	0.34	9.3	1.38	20.2

Table 2: Main physical property indexes of PO. 42.5 composite silicate cement.

Materials	Coagulation time (min)		Consistency (%)	Specific surface area (m^2·kg^{-1})	Compressive strength (MPa)		Shear strength (MPa)	
Cement	Initial condensation	Final condensation	Water quantity method	≥320	3 d	28 d	3 d	28 d
	13.7	18.6	25.4	337	25.7	53.8	6.1	7.9

Specific surface area is the total surface area of cement powder per unit mass.

remains low, which is not conducive to the diffusion of the slurry. We determined that the grouting requirements were met at the water-cement ratio of 1.0. During the grouting process, the slurry was stirred on-site with an electric mixer and measured with a hydrometer to ensure that the properties of the slurry met the design requirements.

Equipment such as drilling machine, grouting machine, and grouting pressure gauge was used in the field splitting grouting test (Figure 3). The type and specification of grouting equipment are presented in Table 3. There were three opening directions for each layer of the steel pipe in the grouting section, which were arranged in a plum-shaped arrangement; the angle included between the directions was 120°. According to hole depth, the steel flower tube was divided into three sections, and the threaded connection was used for easy disassembly. The grouting method was adopted in layers and sections from bottom to top. The assembled grouting pipe was placed in the drilled grouting hole. The top of the grouting pipe was connected to the grouting pump.

After the grouting equipment was installed, the grouting machine was started to start grouting, as shown in Figure 4. During the grouting process, the grouting amount and

(a) (b) (c)

Figure 3: Grouting equipment: (a) drilling machine; (b) grouting pump; (c) air compressor.

Table 3: Grouting equipment.

Equipment name	Type	Specifications
Grouting machine	ZKSY90-125	0–16 MPa
Drilling machine	JK730-2	2200 × 1400 × 3000
Air compression machine	XA57E	4.2 m^3/min
Alternator machine	KC-300	300 kW

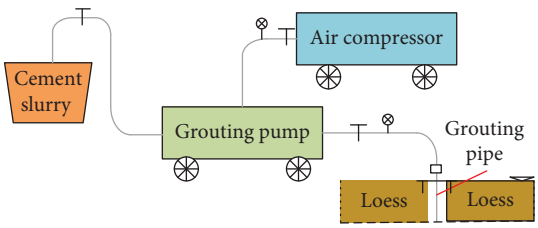

Figure 4: Grouting system.

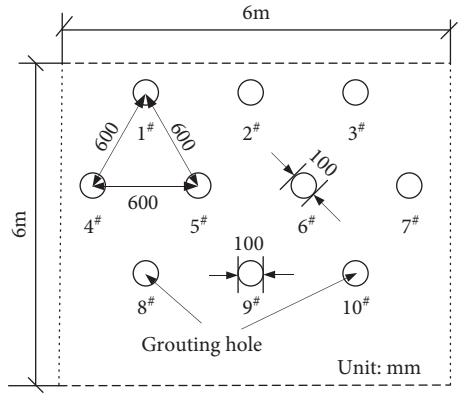

Figure 5: Grouting hole arrangement diagram.

grouting pressure of each grouting hole were monitored and recorded continuously. When the grouting amount reached the design value, grouting in the soil layer section was stopped, the grouting pipe was reassembled, and the abovementioned grouting process was repeated until grouting in the uppermost soil layer was completed. When the grouting was carried out, it was ensured that the other parts were sealed grouting pipes except this layer.

The size of the grouting site was 6 m × 6 m, the drilling depth of the grouting hole was 9 m, the diameter of the drilling hole was 100 mm, and hole spacing was 600 mm, as shown in Figure 5. To prevent grout mixing in each grouting hole, the principle of hole spacing grouting was adopted. After the completion of single hole grouting, grouting was carried out in every other hole. The grouting sequence was holes 1, 3, 9, and 11, holes 2, 5, 8, and 10, and finally, holes 6 and 7. The loess around the hole absorbed the water in the slurry, and the slurry infiltrated and diffused in the soil. After grouting, to prevent the occurrence of hollow piles at the top of the grouting pile, it was necessary to replenish the grouting after some time; each hole was grouted 4 or 5 times to ensure the integrity of the split grouting pile.

3.3. Static Load Test. The static load test equipment mainly included a 200 t hydraulic jack, 50 t hydraulic jack, small steel beam, circular pressure plate, and dial indicator, along with some other measuring equipment, as shown in Figure 6. To ensure the accuracy of the measurement results during the test, all equipment was checked before the tests. The measuring range of the dial indicator was 1 cm, accuracy was 0.001 mm, area of the pressure bearing plate was 0.64 m^2, and thickness was 30 mm.

The static load test adopted the reaction force stacking method. By setting up a test platform centered on the test pile, stacking sand bags, concrete counterweights, steel ingots, and so on, and by pressurizing using jacks, vertical pressure was applied on the test pile to check whether the bearing capacity of the test pile satisfied the design requirements [18], as shown in Figure 7. The counterweight was a concrete test block. The total weight of the stacking test block was 120 t, the lower part was a 6 concrete block support, and the upper part was supported by three steel beams to ensure a stable reaction force on the jack during the test. Before the test, a 50 cm part of the pile head was removed, the surface of the foundation was leveled, and a 100 mm sand cushion was laid. The load plate was placed on the sand cushion, and then, the jack was placed in the center of the load plate. When placing the bearing plate, the center of the circle was placed on the center of the pile, and the jack was placed on the center of the bearing plate. The upper part of the jack was in contact with the upper steel beam via a steel cushion block, which was placed on the central axis during the placement, and the initial reading of the dial indicator was recorded. This test was loaded in 10 stages, and the loading amount of each stage was 1/10 of the maximum

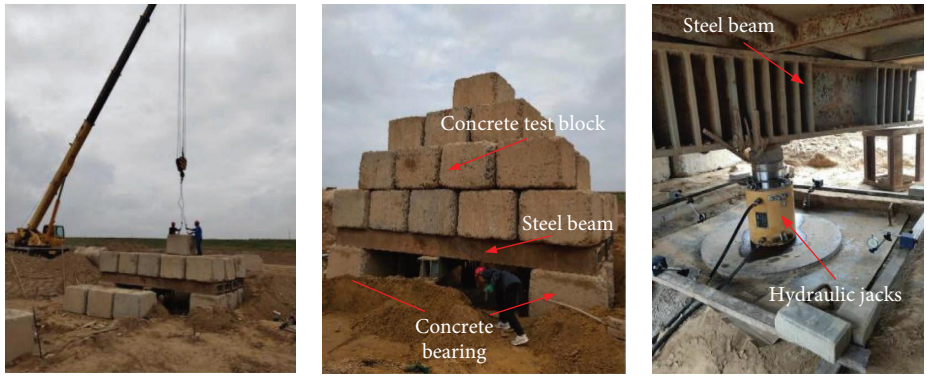

(a) (b) (c)

Figure 6: Test equipment diagram: (a) test block lifting; (b) superstructure; (c) substructure.

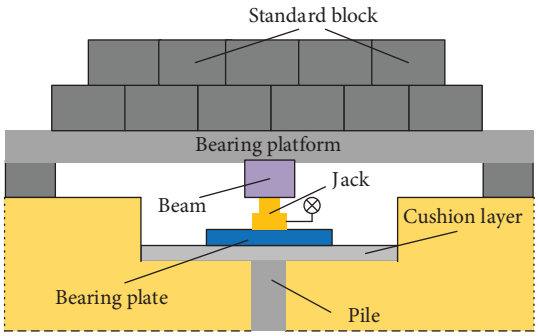

Figure 7: Schematic diagram of reaction force stacking method.

Figure 8: Heavy-duty penetration test.

loading amount [19]. After each loading stage, the settlement of the load plate was recorded at intervals of 5, 10, 15, 15, 15, 30, and 30 min. When the settlement rate reached <0.1 mm/h, the next level of load was applied; otherwise, we continued to observe every 30 min. When the settlement increased sharply and there was an obvious bulge around the bearing plate, the accumulated settlement of the bearing plate was >6% of its width or diameter, and the maximum loading pressure was >2 times the design pressure value. In the previous cases, the test was terminated.

Before the single-pile bearing capacity was tested, the maximum loading capacity of the natural foundation was determined. A heavy-duty static probe was used to test the bearing capacity of the natural foundation, as shown in Figure 8. A 63.5 kg center hammer was used to drive the contact probe into the soil with a drop distance of 76 cm; the number of blows at 10 cm was recorded, 5 points were selected for dynamic penetration tests, the number of blows required for each point of 10 cm drop was recorded, the test was stopped when the total drop was 30 cm, and then, the average values of the tests were obtained.

According to the recorded number of hammer blows, the allowable bearing capacity, f_{c0}, of the natural foundation was calculated using formula (1) [20]. The test results and calculation results are shown in Table 4.

$$f_{c0} = aN + b, \tag{1}$$

where f_{c0} is the allowable bearing capacity of the foundation (kPa), N is the average hammering number of heavy penetration, and a and b are the regression coefficients of the empirical formula, $a = 35.96$, $b = 23.8$.

As shown in Table 4, the average allowable bearing capacity of natural foundations was approximately 118 kPa. This single-pile composite foundation static load test was used to measure its ultimate bearing capacity, and the minimum area of the bearing plate used was 0.36 m^2. Therefore, the maximum load was estimated to be 450 kN.

3.4. Analysis of Test Results

3.4.1. Analysis of Bearing Capacity of Single-Pile. Single piles No. 2 and 9 were selected in the test area for single-pile bearing capacity tests, and the load-settlement curves of the test piles were obtained, as shown in Figure 9. As shown in Figure 9, when the load was increased to 100 kN, the top settlement of single piles No. 2 and 9 reached 17.42 mm and 15.05 mm, respectively. At this time, the curve showed significant settlement, indicating that the bearing capacity of the single pile had reached the ultimate load at this time. The ultimate load value was the load of the previous level of steep drop, and the ultimate load was 90 kN. Therefore, the bearing capacity of single piles No. 2 and 9 was 45 kN.

Table 4: Heavy-duty touch record table.

Point location	Number of hammer blows required to descend the i-th 10 cm			Average value	R (kPa)
	$i=1$	$i=2$	$i=3$		
1	3	2	3	2.67	119.81
2	2	2	2	2	95.72
3	2	2	4	3	131.68
4	2	3	4	2.67	119.81
5	2	2	4	2.67	119.81

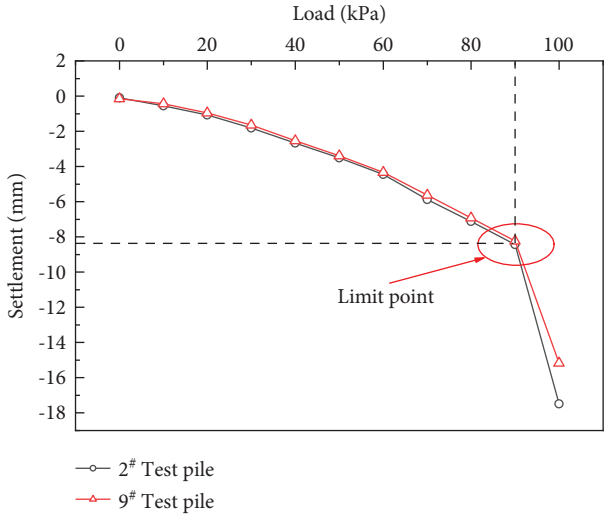

Figure 9: Test pile load-settlement curves for single piles No. 2 and 9.

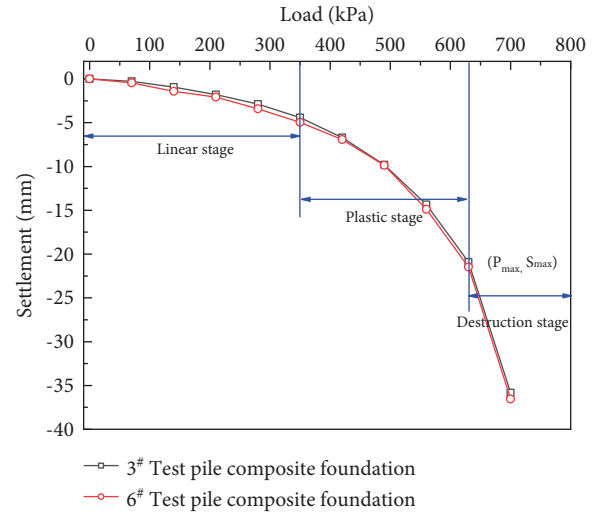

Figure 10: Test pile composite foundation load-settlement curves of single piles No. 3 and 6.

3.4.2. Bearing Capacity Analysis of Single-Pile Composite Foundations. Single piles No. 3 and 6 were selected for static load tests on the single-pile composite foundation, and the load-settlement curve is shown in Figure 10. Figure 10 shows that the change trend of the Q-s curve of the two piles was basically the same, indicating that the bearing capacity of the two single-pile composite foundations was almost the same. With the increase in applied pressure, the foundation settlement was in the linear change stage at 0–350 kN, and the deformation of piles and soil was the same, sharing the upper load of the plastic deformation stage occurred at 350–630 kN. After the load reached 630 kN, the curve showed a "steep drop" trend, showing that the pile body and its branches were damaged, and the original state of the pile and the soil changed completely; this stage was called the failure stage. Thus, the settlement change of each single-pile composite foundation was divided into three stages, namely, linear, plastic, and failure. Therefore, the ultimate bearing capacity of the single-pile composite foundation was determined to be 630 kPa.

3.4.3. Analysis of Single-Pile Excavation Results. After the static load test was complete, the split grouting pile of No. 7 was excavated on-site to observe the pile forming mechanism of the split grouting pile, as shown in Figure 11. A tape measure was used to measure the pile core and splitting branches after excavation; the pile body itself was cylindrical, ideal splitting occurred on the side wall of the grouting hole, the splitting direction was the opening position of the grouting pipe, thick branches were formed in both directions, and the split branches were in a "sheet" shape. The horizontal extension distance of the branch was approximately 37 cm, and the maximum depth of vertical diffusion near the pile body was 35 cm, which conforms to the law of slurry diffusion. The closer it was to the pile body, the greater the pressure, the more obvious the diffusion in the soil body, and a more obvious effect on the improvement of the bearing capacity of the foundation.

4. Settlement Calculation

According to the characteristics of the split grouting pile composite foundation, the calculation of the total settlement [11] was divided into compression of the reinforcement area and compression of the bottom layer, as shown in Figure 12.

4.1. Settlement Calculation of Reinforcement Area

4.1.1. Composite Modulus Method. In this calculation method, the pile body and the soil body were regarded as a whole, and the composite modulus of the composite foundation was obtained using the weighted average

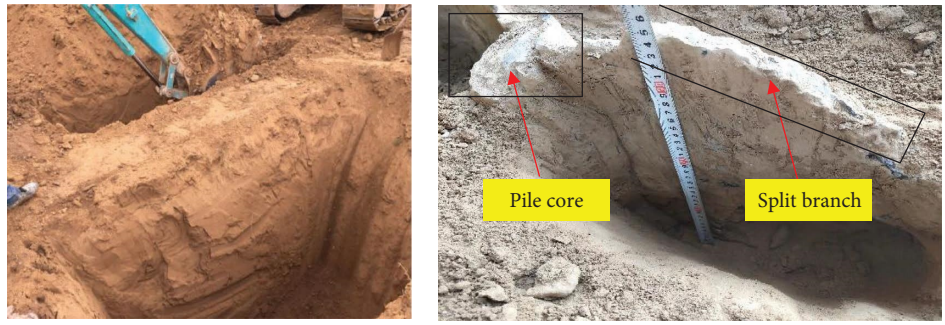

(a) (b)

Figure 11: Site excavation: (a). Pile excavation; (b). Pile composition.

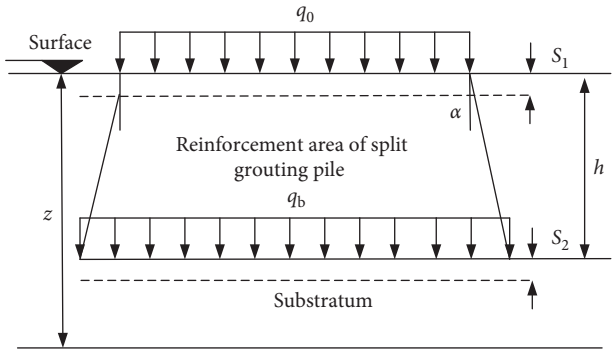

Figure 12: Schematic diagram of composite foundation.

method. Therefore, the compressive modulus of a composite body is calculated as follows:

$$E_{csi} = mE_{ps} + (1 - m)E_{si}, \tag{2}$$

$$m = \frac{d^2}{d_e{}^2}, \tag{3}$$

where E_{si} is the compressive modulus of the i-th layer soil, E_{ps} is the compressive modulus of the pile, m is the replacement rate of the composite foundation, d is the diameter of the pile, and d_e is the equivalent reinforcement area of a single pile.

The soil in the reinforcement area was divided into n layers, and the layered sum method (formula (4)) was used to calculate the settlement of the reinforcement area of the composite foundation.

$$S_1 = \sum_1^n \frac{\Delta p_i}{E_{csi}} H_i, \tag{4}$$

where Δp_i is the additional stress in the upper part of the i-th layer of soil in the reinforcement area, H_i is the thickness of the i-th layer of soil, and E_{csi} is the compression modulus of the i-th layer of soil.

The calculated parameters, namely, $l = 9$ m, $S = 0.6$ m, $d = 0.1$ m, and $E_{ps} = 1.5 \times 10^7$ kPa were substituted into formulas (2) and (4) and were summarized, as shown in Table 5.

4.1.2. Stress Correction Method. In the calculation process of the proposed method, only the soil between the piles was considered, and the layered sum method was used to calculate the compression settlement of the natural foundation; thereafter, according to the specific conditions and corrections, the settlement of the reinforcement area was determined as follows:

$$\begin{aligned} S_1 &= \mu_s \sum_1^n \frac{\Delta p_{si}}{E_{si}} H_i = \mu_s S_1{}', \\ \mu_s &= \frac{1}{1 + m(n-1)}, \end{aligned} \tag{5}$$

where Δp_i represents the additional stress on the top of the i-th layer of soil without reinforcement, μ_s represents the stress correction coefficient, n is the pile-soil stress ratio, and m represents the replacement rate.

In the calculation, the compressive modulus of soil was corrected by the coefficient. The compressive moduli of the two layers of soil were $E_{s1} = 3.3 \times 10^4$ kPa and $E_{s2} = 4.16 \times 10^4$ kPa. The additional stress on the upper part of the soil was the same as that calculated in Table 4. According to the numerical simulation results in Section 4, $n = 24.69$, and the settlement of the soil layer of the natural foundation under the load was $S_1{}' = 22.835$ mm. The correction, given the settlement in the reinforced area, was $S_1 = 8.22$ mm.

4.2. Settlement Calculation of Lower Lying Layer. The substratum of the composite foundation adopted the layered sum method to calculate the settlement using the following formula:

$$S_2 = \sum_{i=1}^n \frac{e_{1i} - e_{2i}}{1 + e_{1i}} H_i = \sum_{i=1}^n \frac{\Delta p_{si}}{E_{si}} H_i, \tag{6}$$

where for the i-th soil layer, Δs_i is the compression, e_{1i} is the pore ratio of the average value of the self-weight stress and the additional stress, H_i is the thickness, Δp_i is the sum of the additional stress of soil at the top and bottom of the i-th soil layer, and E_{si} is the compressive modulus of the i-th soil layer.

Table 5: Summary of calculation results.

Number of layers	Depth from surface z (m)	Additional stress in soil p (kPa)	Soil thickness Hi (m)	Composite modulus E_{cs} (MPa)	Settling volume $S1$ (mm)
0	0	563	1	3.57×10^5	
1	1	261.25	1	3.57×10^5	
2	2	95	1	3.57×10^5	
3	3	45	1	3.57×10^5	
4	4	25.5	1	3.57×10^5	
5	5	16.75	1	3.68×10^5	
6	6	12.5	1	3.68×10^5	
7	7	7.5	1	3.68×10^5	
8	8	5	1	3.68×10^5	
9	9	5	1	3.68×10^5	
$\sum$					3.073

The stress-diffusion method was used to calculate the load on the upper part of the substratum, and the calculation was as follows:

$$P_b = \frac{LW\mathrm{p}}{(L + 2H\tan\beta)(D + 2H\tan\beta)}, \quad (7)$$

where L is the length of the upper foundation, W is the width of the foundation, H is the depth of the reinforced area, p is the size of the upper load, and β is the pressure diffusion angle.

The calculation of the upper load of the substratum was carried out under the single pile. The depth of the reinforcement zone was 9 m. From the compressive modulus of the soil, the ratio of the compressive modulus of the adjacent soil at the bottom of the pile reinforcement was determined to be $E_{s1}/E_{s2} = 0.922 < 3$. When the pressure diffusion angle was selected, it was regarded as a homogeneous soil body for calculation. The calculation parameters, namely, $L = 0.8$, $W = 0.8$, $P = 563$ kPa, were substituted into formula (7) to calculate the additional stress at the bottom of the pile at $p_b = 310$ kPa, which was calculated using the layered sum method; the settlement calculation is shown in Table 6.

According to Table 6, when calculations were carried out for the third layer of soil, it conformed to the determination of the foundation compression settlement depth, $\sigma_{z3} = 22.32 < 0.2\ \sigma_{c3} = 39.76$ mm; the calculated depth was 12 m from the top of the pile, and the total calculated settlement of the substratum was $S_2 = 16.634$ mm.

The settlement results of the composite foundation of the split grout pile were compared with the field test results, as shown in Table 7. The calculation of settlement of the split grouting composite foundation using the composite modulus method had a small error of 6.4% compared with the test results; the calculation results using the stress correction method had a larger error with the field test results, which cannot satisfy the requirements of practical engineering applications. Therefore, the composite modulus method was used for calculating the settlement of the composite foundation of slurry piles in the field.

5. Numerical Simulation

5.1. Single-Pile Composite Foundations

5.1.1. Model Building. A finite element model of the split grouting pile composite foundation was established by software ABAQUS. The Mohr–Coulomb model was used for the foundation loess. The size of the soil model was 10 m × 10 m × 22 m, which was divided into three layers from top to bottom. The lengths of the piles and branches were the same as the results obtained for the on-site excavation. The pile body and the branches were all selected from the linear elastic model. The load plate (diameter = 680 mm, thickness = 30 mm) was completely rigid; the model material parameters are shown in Table 8.

For contact between the load plate and the soil at the top of the pile, the tangential direction was frictionless, the normal direction was hard contact, and the friction coefficient was 0.35. Branches are defined as embedded constraints in the soil and are set as built-in area constraints. During the loading process, the pile body was prevented from spreading and deforming, the bottom surface of the soil body was constrained by displacement in three directions, that is, $U_1 = U_2 = U_3 = 0$, and the top was not constrained to facilitate loading and settlement. The pile body and the pressure plate were relatively small in volume relative to the soil body, and only the approximate global size was defined. The whole structure was divided into 762 and 768 units; the mesh division is shown in Figure 13.

5.1.2. Pile Shaft Force Analysis. The calculation results of the axial force of the pile body were obtained, and the distribution diagram of the axial force of the pile body was drawn (Figure 14). The axial force of the pile body exhibited a stepped attenuation trend. When the pile body load was transmitted, the branches could bear part of the load, decreasing the pile body stress, and thereby improving the overall bearing capacity. During loading, the stress at the top of the pile was the same as the axial force at the top of the pile. With the increase in depth, the branch of the pile body could bear part of the load, and the force gradually decreased

Table 6: Settlement calculation table.

Depth z_i (m)	Self-weight stress σ_c (kPa)	Additional stress σ_z (kPa)	Average value of self-weight stress (kPa)	Average value of additional stress (kPa)	Settlement S (mm)
0	0	310			
1	161.9	129.58	80.95	300.74	6.523
2	180.2	47.12	171.05	259.4	5.62
3	198.8	22.32	189.5	224.22	4.484
$\sum$					16.634

Table 7: Comparison of settlement calculation results.

Category	Composite modulus method	Stress correction method	Test results
Settlement (mm)	19.707	24.845	18.59
Error (%)	6.4	33.3	0

Table 8: Model material parameters.

Soil layer	Thickness h (m)	Density ρ (t·m^3)	Modulus of elasticity E (MPa)	Poisson's Ratio ν	Angle of internal friction ϕ (°)	Cohesion c (kPa)
Backfill layer	4	1.76	33	0.3	8	15
Loess-like silt	7	1.83	46.1	0.35	15	36
Malan loess	11	1.86	50	0.32	17	32
Pile	—	1.76	1.5×10^4	0.21	—	—
Load plates	—	7.85	2.06×10^8	0.30	—	—

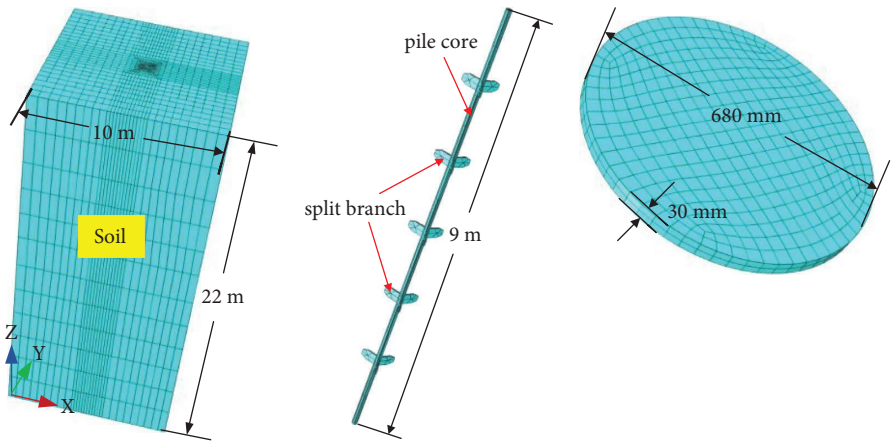

Figure 13: Finite Element Model: (a) soil model; (b) pile model; (c) bearing plate model.

and tended to zero at the end. After the depth reached 4.5 m, the axial force attenuated rapidly, and the load on the top of the pile accounted for 83.9%, 82.4%, 81.4%, 80.6%, 79.4%, 78.4%, 77.6%, 65.5%, 58.5%, and 52.4%, indicating that the upper part of the pile could bear more than half of the load of the pile, forming the main bearing part, and the proportion of bearing decreased with the increase in load.

5.1.3. Analysis of Pile Lateral Friction Resistance. The variation trend of the side friction resistance of the split grouting pile with depth was drawn as a curve (Figure 15). The lateral friction resistance distribution of the split grouting pile was similar to that of other rigid piles. At the outer curve of the edge, the lateral friction resistance of the pile showed a trend of first increasing, then decreasing, and then increasing. When acting, the side friction resistance was negative (at 0.1 l) because the distance between the upper part of the soil and the bearing plate at this depth were similar, the soil within the range was limited, and the soil moved downward relative to the pile. After the soil works, the stress was fully transferred down to the deeper part, and the maximum lateral friction resistance was at the 0.5 l position. At the same time, the stress of the side friction

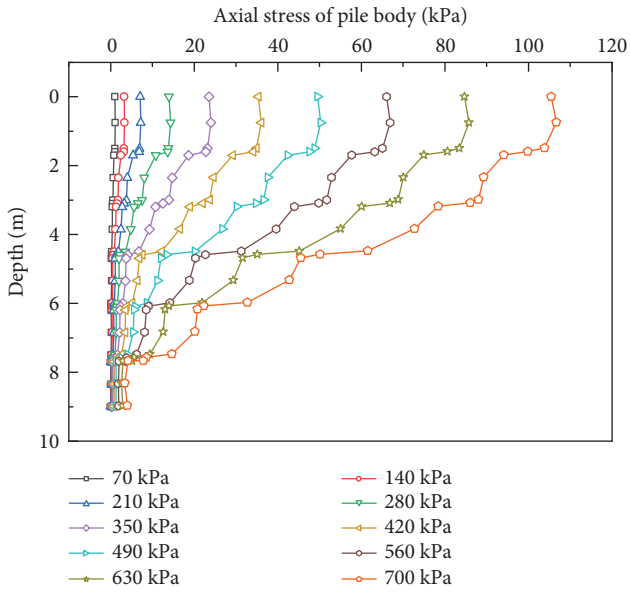

Figure 14: Pile axial force distribution diagram.

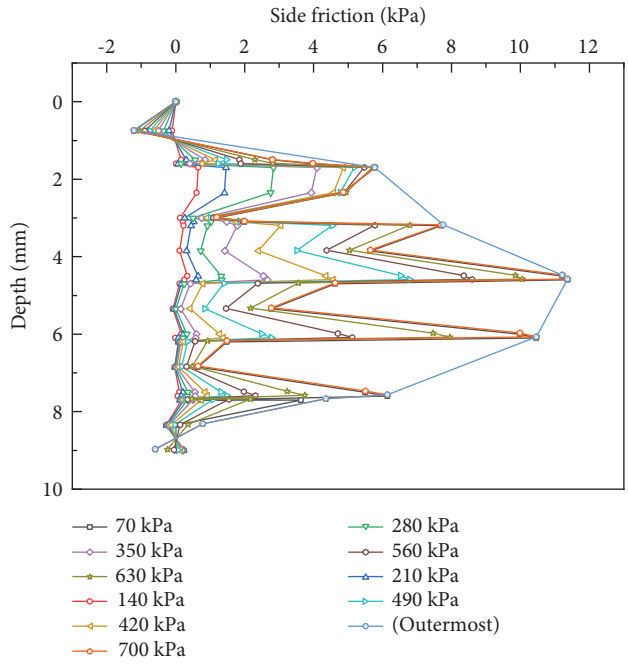

Figure 15: Pile side friction resistance diagram.

resistance decreased during the change process. This was attributed to the existence of the branches that shared the side friction resistance, because of which, the maximum peak value of the side friction resistance was transmitted to the deeper part of the pile body, mitigating the settlement of the pile body.

5.1.4. Single-Pile Composite Foundation Settlement Analysis. The displacement cloud diagram of the split grouting pile composite foundation is shown in Figure 16. Figure 16(a) shows the stress displacement at the top of the composite foundation. There is obvious displacement under the pressure plate, the overall diffusion trend is centered on the pressure plate, and different displacement diffusion trends are shown under different stress states. The maximum part of intermediate displacement was the range of circular pressing plate. Taking the single pile as the center, the influence range of the load was approximately 3 m. When designing the split grouting pile composite foundation, it is crucial to choose the optimal pile spacing. Figure 16(b) shows the soil displacement along the z-axis. Along the depth direction, the displacement showed obvious stratification. The displacement transmission of the upper part was relatively uniform, and it started decreasing at the bottom 3/4 part, showing different settlement sizes under different stress states. Figure 16(c) shows that the overall displacement of the pile top was relatively large. The pile displacement was mainly concentrated in the upper part. For branches, the settlement was accompanied by compression settlement of the pile and soil, the settlement of the upper branch was larger, and the settlement of the branch decreased with increase in depth. When carrying out stress tests, the pile body could bear a large force, and the settlement of the pile body was greater than that of the surrounding soil. Therefore, for the branches, the settlement near the end of the pile body was greater than that at the far ends.

Numerical simulation results of the composite foundation settlement were compared with the field test results, as shown in Figure 17. The settlement results of the two groups increased with the increase in the load of the pressure plate, and the change trend was nearly consistent. At a load of 400 kPa, the measured value of settlement rate was greater than the simulated value, and at load of 600 kPa, the simulated value showed a consistent decreasing trend and not a sudden and steep drop stage. This was because soil acted as a uniform and ideal elastic-plastic body during the simulation, and it exhibited relatively regular changes during stress and fracture. Compared with the field test, the branch formation was more uncontrolled. When the branch was damaged by shear, the settlement increased rapidly and the slope increased, which led to a more idealized finite element simulation result. Analysis of the results showed that the change curve was relatively close, and the relative error was within 5%, indicating that the selected parameters were more consistent with the field test data and are thus suitable for providing theoretical guidance for the field test.

Luo et al. [21] determined that the ultimate bearing capacity of the split grouting pile single-pile composite foundation was 716 kPa when the pile diameter was 160 mm and the pile spacing was 800 mm. Compared with the composite foundation with pile diameter of 100 mm and pile spacing of 600 mm in this study, the ultimate bearing capacity of the single-pile composite foundation increased by 15.2%. Compared with the pile spacing, pile diameter was highly sensitive to the bearing capacity of composite foundation. Figure 17 shows that the linear change stage of the composite foundation with large pile diameter was long, and the settlement of composite foundation was obviously small. Therefore, in the design of the composite foundation

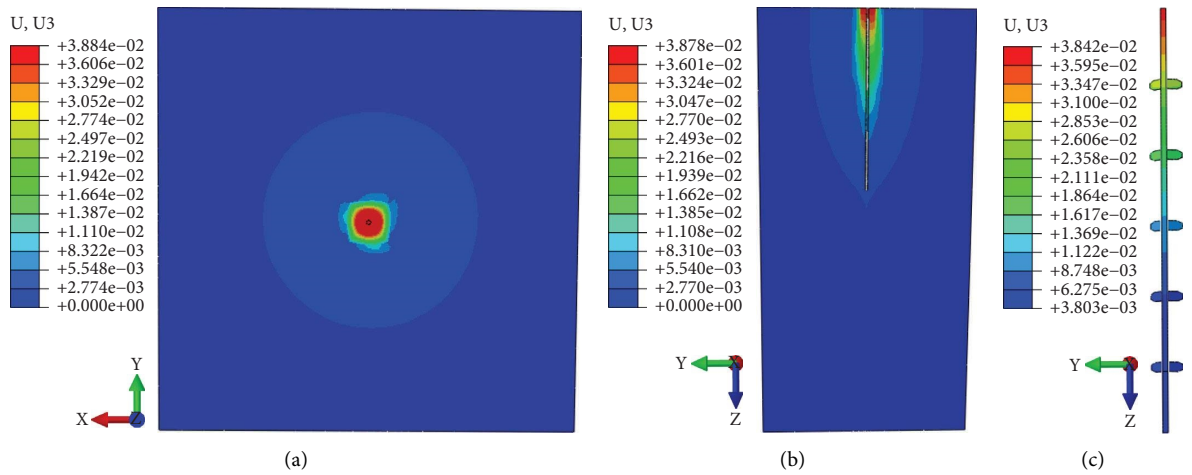

Figure 16: Composite Foundation Displacement: (a) top displacement; (b) vertical section; (c) pile displacement.

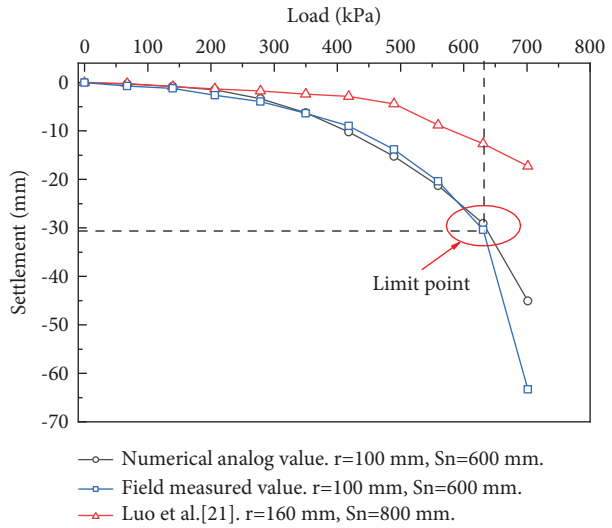

Figure 17: Comparison of measurement results and those of numerical simulations.

with split grouting piles, it was more effective to consider selecting a larger pile diameter than reducing the pile spacing.

5.2. Multi Pile Group Composite Foundation Model

5.2.1. Model Building. The pile material and soil material parameters of the split grouting multipile composite foundation model were the same as that of the single-pile composite foundation model. Soil model size was $10 \times 10 \times 22\ m^3$, and bearing plate model size was $1.7 \times 1.7 \times 0.3\ m^3$. The pile arrangement form was a regular triangle, the number of piles was 8, and pile spacing was 0.6 m, as shown in Figure 18. For contact between the load plate and soil at the top of the pile, the tangential direction was still frictionless, and the normal direction was still hard contact. Restraining was used around the load plate to prevent force diffusion of the load plate. To ensure contact between the pile and soil, surface-to-surface contact was still used, with a friction coefficient of 0.35. The branch adopted the built-in area, and the soil was inside the area.

5.2.2. Settlement Analysis of Multi Pile Composite Foundation. The calculated displacement nephograms of the composite foundation of split grouting multi pile are shown in Figure 19. As shown in Figure 19(a), the soil settlement gradually decreased from the pile outward diffusion, and the settlement at the contact between the top of the composite foundation and the bearing plate was the largest, and it decreased with the increase in depth. The contact area between the middle soil under the action of the bearing plate was the largest; thus, the settlement of the middle soil was the largest, and the settlement of the surrounding soil was relatively decreased. Due to the compaction of the pile bottom with the soil, the contact part had a large settlement, and the downward transmission gradually decreased, with a transmission depth of approximately 4 m. Figure 19(b) shows that the displacement at the top of the

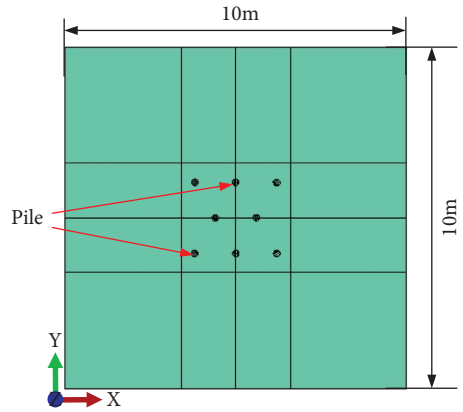

Figure 18: Pile distribution of pile group composite foundation model.

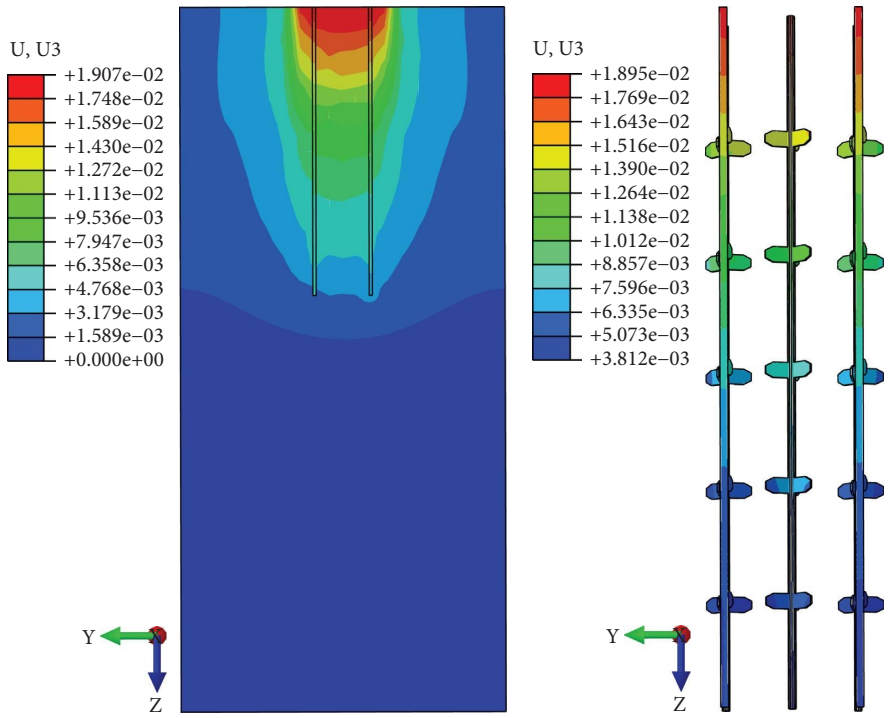

Figure 19: Multipile Composite Foundation Displacement: (a) pile-soil settlement section; (b) pile displacement.

pile was relatively large, while the displacement at the bottom was relatively small. The overall displacement of the pile was mainly concentrated at 1/2 of the pile. The overall displacement of the pile was consistent with soil. At the same depth, the displacement of the middle pile was the largest, and it was slightly larger than that of the side center pile. The settlement of the corner pile was the smallest. Although the force on the corner pile was large, the force transmission area of the upper load was small, resulting in a small settlement. The settlement deformation law of the branch was consistent with the pile and soil. For the action surface at the same depth, the settlement of the central branch was larger, the settlement of the diffusion around gradually decreased, and the settlement of the outer side reached the minimum value. On the same vertical action surface, the settlement of the branch was obvious, and it played a key role in reducing the settlement of the composite foundation. Because the branch blocks the upper load, the cumulative settlement of the soil between the piles was reduced, thus strengthening the coordination between the pile and soil.

The numerical simulation results of settlement of multipile composite foundation were compared with the field test results, as shown in Figure 20. The change trend of the two curves was basically the same. Compared with the settlement of the single-pile composite foundation, the overall change was no longer smooth, indicating that the

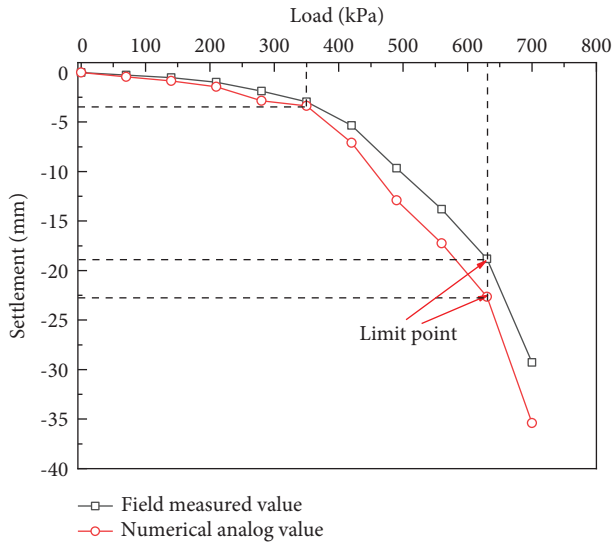

Figure 20: Comparison of numerical simulation and measured results.

interaction between pile and soil of pile groups was more complex. When the load was <350 kPa, the measured settlement was close to the simulation value, indicating that the results of the numerical model were close to the field test results in the linear deformation stage of composite foundation. When the load continued to increase, the relative error between the two increased, and the increase rate of numerical simulation value was larger than the increase in the field test value. This was because the pressure during grouting was not easy to control, resulting in differences in the sizes of each layer of branches. Therefore, the development speed of site foundation settlement was slow, while the numerical model was more ideal, and the overall settlement change rate was fast. After the load reached 630 kPa, the test curve showed a steep drop stage, indicating that the composite foundation had reached the limit state. Analysis of the overall results showed that the two curves did not differ considerably. If numerical simulation is adopted for designing split grouting pile composite foundations, it should be more conservative so as to provide references for test designs.

6. Conclusion

To study the effect of strengthening loess foundations with split grouting piles, the settlement characteristics of composite foundation formed were analyzed, the methods of field test, theoretical calculations, and numerical simulations were used, and the following conclusions were obtained:

(1) Compared with the natural loess foundation, the split grouting pile composite foundation has nearly 3 times higher bearing capacity, which shows that the bearing capacity of the loess foundation can be significantly improved by using split grouting piles, proving the effectiveness of the split grouting pile to strengthen the loess foundation.

(2) The composite modulus method and the stress correction method were used to calculate the composite foundation settlement, and compared with the field measurement results, the error with the composite modulus method was only 6.4%, while the error of the stress correction method was relatively large. Therefore, the composite modulus method was more suitable for the theoretical calculation of split grouting pile composite foundation and can be used to predict the foundation settlement when split grouting piles are used to strengthen the loess foundation.

(3) According to the pile forming mechanism, the finite element model of the split grouting pile composite foundation was established and loaded, and the axial force of the pile shaft presents a stepped attenuation trend because the branch will bear part of the load. Also affected by the branch, the stress reduction occurred in the change process of the lateral friction resistance. Therefore, considering that the branch has a large impact on the pile performance, enabling reasonable control of the formation of branches during fracturing grouting can be of great significance in future research.

(4) The composite foundation settlement simulation results were compared with the field test results. The load-settlement curves of the two methods were nearly consistent, and the relative error was controlled within 20%. Thus, the parameters and modeling methods selected in the simulation process were considered reasonable, which proves that the split grouting pile composite foundation model can provide theoretical guidance for designing split grouting piles and can predict the deformation of the split grouting pile composite foundations in practical engineering applications. Moreover, the influence of foundation settlement on the stability of superstructure can be reduced.

Data Availability

The data used to support the findings of this study are available from the corresponding authors upon request.

Conflicts of Interest

The authors declare that they have no conFIicts of interest.

Acknowledgments

The authors would gratefully like to acknowledge the support provided by the National Natural Science Foundation of China (nos. 52178216).

References

[1] M. Qiu, X. Shao, Y. Zhu, H. H. Hussein, and Y. Liu, "Tensile and flexural tests on ultrahigh performance concrete grouted

sleeve connection," *Structural Concrete*, vol. 2022, Article ID 17517648, 2022.

[2] A. Rezamand, M. Afrazi, and M. Shahidikhah, "Study of convex corners' effect on the displacements induced by soil-nailed excavations," *Journal of Advanced Engineering and Computation*, vol. 5, no. 4, pp. 277–290, 2021.

[3] V. Nowroozi, H. Hashemolhosseini, M. Afrazi, and E. Kasehchi, "Optimum design for soil nailing to stabilize retaining walls using FLAC3D," *Journal of Advanced Engineering and Computation*, vol. 5, no. 2, pp. 108–124, 2021.

[4] Z. Li, S. Li, H. Liu, Q. Zhang, and Y. Liu, "Experimental study on the reinforcement mechanism of segmented split grouting in a soft filling medium," *Processes*, vol. 6, no. 8, p. 131, 2018.

[5] M. Afrazi and M. Yazdani, "Determination of the effect of soil particle size distribution on the shear behavior of sand," *Journal of Advanced Engineering and Computation*, vol. 5, no. 2, pp. 125–134, 2021.

[6] R. Lang and A. Yang, "A quasi-equal strain solution for the consolidation of a rigid pile composite foundation under embankment loading condition," *Computers and Geotechnics*, vol. 117, Article ID 103232, 2020.

[7] X. Cheng, W. Jing, C. Yin, and C. Li, "Stability parameter analysis of a composite foundation of an oil storage tank in a loess area treated with compaction piles," *Soils and Foundations*, vol. 58, no. 2, pp. 306–318, 2018.

[8] W. Zhu, G. Ye, L. Gu, and F. Zhang, "1g model test of piled-raft foundation subjected to vibration load and its simulation considering small confining stress," *Soil Dynamics and Earthquake Engineering*, vol. 156, Article ID 107212, 2022.

[9] J. Gao, Y. Zhang, C. Wang, and C. Yuan, "Behavior characteristics of geosynthetic-encased stone column under cyclic loading," *Transportation Geotechnics*, vol. 28, Article ID 10554, 2021.

[10] Y. Yi, S. Liu, and A. J. Puppala, "Bearing capacity of composite foundation consisting of T-shaped soil-cement column and soft clay," *Transportation Geotechnics*, vol. 15, pp. 47–56, 2018.

[11] L. Zhang, M. Zhao, C. Shi, and H. Zhao, "Settlement calculation of composite foundation reinforced with stone columns," *International Journal of Geomechanics*, vol. 13, no. 3, pp. 248–256, 2013.

[12] K. Liu, R. Qiu, T. Yan et al., "Model test of clogging effects on composite foundation of geosynthetic-encased steel slag column," *Geotextiles and Geomembranes*, vol. 50, no. 5, pp. 858–867, 2022.

[13] D. J. Useche-Infante, G. M. Aiassa-Martinez, P. A. Arrua, and M. Eberhardt, "Performance evaluation of post-grouted drilled shafts: a review," *Innovative Infrastructure Solutions*, vol. 7, no. 3, pp. 230–323, 2022.

[14] L. N. Ma, S. H. Yan, and R. L. Zhang, "High-speed railway's roadbed consolidation with fracture grouting in collapsible loess area: mechanism and application," *Materials Research Innovations*, vol. 19, no. 6, pp. S6-S111–S6-115, 2015.

[15] Z. Zhang, Z. Shao, X. Fang, and X Liang, "Research on the fracture grouting mechanism and PFC numerical simulation in loess," *Advances in Materials Science and Engineering*, Article ID 4784762, 2018.

[16] J. Niu, Z. Li, W. Gu, and K. Chen, "Experimental study of split grouting reinforcement mechanism in filling medium and effect evaluation," *Sensors*, vol. 20, no. 11, p. 3088, 2020.

[17] M. Zhou, N. Li, L. Zhong, and S. Li, "Experimental study on rock strength of split grouting pile core in collapsible loess areas," *Bulletin of Silicate*, vol. 40, pp. 1147–1153, 2021.

[18] G. Cai, S. Liu, L. Tong, and G. Du, "Assessment of direct CPT and CPTU methods for predicting the ultimate bearing capacity of single piles," *Engineering Geology*, vol. 104, no. 3-4, pp. 211–222, 2009.

[19] The Professional Standards Compilation Group of People's republic of China, *Technical Code for Ground Treatment of Buildings*, China construction industry pubic house, Beijing, China, 2012.

[20] The Professional Standards Compilation Group of People's republic of China, *Specifications for Design of Foundation of Highway Bridges and Culverts*, Ministry of transport of the people's republic of China, Beijing, China, 2019.

[21] X. B. Luo, Y. Song, and Q. M. Guo, "Split grouting test and foundation reinforcement application in collapsible loess area in Northwest China," *Journal of Hunan University*, vol. 48, pp. 52–60, 2021.